Opto-Electronic Advances

Supplementary information

November 2023, Vol. 6, No. 11

DOI: 10.29026/oea.2023.230140

Photonic integrated neuro-synaptic core for convolutional spiking neural network

Shuiying Xiang[1]*, Yuechun Shi[2]*, Yahui Zhang[1], Xingxing Guo[1], Ling Zheng[3], Yanan Han[1], Yuna Zhang[1], Ziwei Song[1], Dianzhuang Zheng[1], Tao Zhang[1], Hailing Wang[4], Xiaojun Zhu[5], Xiangfei Chen[6], Min Qiu[7], Yichen Shen[8], Wanhua Zheng[4] and Yue Hao[1]

[1]State Key Laboratory of Integrated Service Networks, State Key Discipline Laboratory of Wide Bandgap Semiconductor Technology, Xidian University, Xi'an 710071, China; [2]Yongjiang laboratory, No. 1792 Cihai South Road, Ningbo 315202, China; [3]The School of Communications and Information Engineering, Xi'an University of Posts and Telecommunications, Xi'an 710121, China; [4]Laboratory of Solid-State Optoelectronics Information Technology, Institute of Semiconductors, Chinese Academy of Sciences, Beijing 100083, China; [5]School of Information Science and Technology, Nantong University, Nantong 226019, China; [6]The College of Engineering and Applied Sciences, Nanjing University, Nanjing 210023, China; [7]Key Laboratory of 3D Micro/Nano Fabrication and Characterization of Zhejiang Province, School of Engineering, Westlake University, Hangzhou 310024, China; [8]Lightelligence Group, Hangzhou 311121, China.

*Correspondence: SY Xiang, E-mail: syxiang@xidian.edu.cn; YC Shi, E-mail: yuechun-shi@ylab.ac.cn

This file includes:

Supplementary information for this paper is available at https://doi.org/10.29026/oea.2023.230140

Section 1: Time-dependent traveling wave model of DFB-SA laser

The rate equations for the carrier density in the gain region $N_1(z,t)$ and SA region $N_2(z,t)$, and the coupled-mode equations for the slowly varying envelopes of the forward traveling wave $F(z,t)$ and backward traveling wave $R(z,t)$ can be expressed as follows[S1–S3],

$$\frac{1}{v_g}\frac{\partial F(z,t)}{\partial t}+\frac{\partial F(z,t)}{\partial z}=\left[\frac{\Gamma g_{1,2}(z,t)-\alpha_s}{2}-\mathrm{i}\delta(z,t)\right]F(z,t)-\mathrm{i}\kappa R(z,t)+s_F\ , \tag{S1}$$

$$\frac{1}{v_g}\frac{\partial R(z,t)}{\partial t}-\frac{\partial R(z,t)}{\partial z}=\left[\frac{\Gamma g_{1,2}(z,t)-\alpha_s}{2}-\mathrm{i}\delta(z,t)\right]R(z,t)-\mathrm{i}\kappa F(z,t)+s_R\ , \tag{S2}$$

$$\frac{\partial}{\partial t}N_1(z,t)=\frac{I_G}{eV}-AN_1(z,t)-BN_1(z,t)^2-CN_1(z,t)^3-g_1(z,t)v_gS(z,t)\ , \tag{S3}$$

$$\frac{\partial}{\partial t}N_2(z,t)=\frac{I_{SA}}{eV}-AN_2(z,t)+g_2(z,t)v_gS(z,t)\ , \tag{S4}$$

where κ represents grating coupling coefficient, v_g is group velocity, Γ denotes the optical confinement factor, s_F and s_R denote the spontaneous emission noises. I_G and I_{SA} represents the bias current of gain and SA region, respectively. Note, for the SA region, the grating coupling term and spontaneous emission noise terms should be removed in Eqs. (S1–S2). V represents the active region volume of the gain and SA regions, respectively. e is electron charge. $g_1(z,t)$ is the material gain of gain region, and $g_2(z,t)$ represents the material absorption coefficient of the SA region.

Specifically, in Eq. (S4), the first term on the right-hand side represents the effect of reverse voltage of the SA region. Note that, there is no direct and simple method to introduce the reverse voltage in the rate equation. Thus, we introduce a reverse bias current I_{SA} to be equivalent to the effect of reverse voltage for simplicity. The second term denotes the depletion of carrier due to the carrier lifetime, and the third term account for the increase of carrier due to the absorption.

Here, the $g_1(z,t)$can be expressed as,

$$g_1(z,t)=\frac{g_N\ln[N_1(z,t)/N_T]}{1+\varepsilon S(z,t)}\ . \tag{S5}$$

The material absorption coefficient of the SA region $g_2(z,t)$ can be phenomenologically introduced as

$$g_2(z,t)=\alpha_0-B_0[N_2(z,t)-N_0]\ , \tag{S6}$$

where $\alpha_0=1.5\times10^6\ \mathrm{m}^{-1}$, $B_0=9\times10^{-18}\ \mathrm{m}^2$, $N_0=0.75\times10^{24}\ \mathrm{m}^{-3}$.

The variables $\delta(z,t)$and $S(z,t)$ denote the detuning factor and photon density which are given, respectively, by ref.[S1–S3]:

$$\delta(z,t)=\frac{2\pi}{\lambda_0}n_{\mathrm{eff}}(z,t)-\frac{\pi}{\Lambda}\ , \tag{S7}$$

$$S(z,t)=\frac{\Gamma n_{\mathrm{eff}}L\sqrt{\varepsilon_0/\mu_0}}{2v_gVh\nu}(|F(z,t)|^2+|R(z,t)|^2)\ , \tag{S8}$$

where λ_0 is reference wavelength, and Λ is the grating period. $\lambda_B=2n_{\mathrm{eff}}\Lambda$ is Bragg wavelength. The parameters g_N, N_T, and ε represent the differential gain, transparency carrier density and gain suppression coefficient, respectively. L and V denotes laser cavity length and active region volume. h is Planck constant.

The effective refractive index $n_{\mathrm{eff}}(z,t)$ is given by:

$$n_{\mathrm{eff}}(z,t)=n_{eff0}-\Gamma\alpha_m g(z,t)\frac{\lambda_0}{4\pi}\ . \tag{S9}$$

The noise terms are assumed to be a Gaussian distributed random processes that satisfy:

$$\langle|\tilde{s}(z,t)||\tilde{s}(z,t)|\rangle=2\sqrt{\frac{\mu_0}{\varepsilon_0}}\frac{\gamma\,\Gamma n_{sp}g(z,t)h\nu}{n_{\mathrm{eff}}(z,t)}\delta(z-z')\delta(t-t')\ . \tag{S10}$$

The boundary conditions include the facet reflections and the external injection can be expressed as[S4],

$$F(0,t) = r_{\mathrm{AR}} R(0,t) + t_{\mathrm{AR}} E_{\mathrm{inj}}(t) e^{-\mathrm{i}(\omega_{\mathrm{inj}} - \omega_0)t} \ , \tag{S11}$$

$$R(L,t) = r_{\mathrm{HR}} F(L,t) \ , \tag{S12}$$

where r_{AR} and t_{AR} denotes the reflection coefficient and transmission coefficient of the AR facet, r_{HR} represents the reflection coefficient of the HR facet. $E_{\mathrm{inj}}(t)$ denotes the external optical stimulus signal. ω_{inj} and ω_0 represent the angular frequency of the injected field and the DFB-SA, respectively.

The basic parameters are given in Table S1. With these parameters, we numerically solve the time-dependent traveling wave model with the split-step finite difference method. The whole laser cavity is split to several tens of subsections with a length of $\Delta z = v_{\mathrm{g}} \Delta t$, where Δt denotes the time step.

Table S1 | Basic parameters used in this work[S1–S3].

Symbol	Description	Value
κ	Grating coupling coefficient	1000 m^{-1}
Λ	Grating period	242.0589 nm
λ_{B}	Bragg wavelength	1550 nm
L	Length of the laser cavity	1500 μm
L_{G}	Length of gain section	1480 μm
L_{SA}	Length of SA section	20 μm
w	Width of waveguide	2 μm
d	Thickness of active layer	60 nm
λ_0	Reference wavelength	1550 nm
A	Linear recombination coefficient	1×10^{8} /s
B	Bimolecular recombination coefficient	1×10^{-16} m^3/s
C	Auger recombination coefficient	3.5×10^{-41} m^3/s
α_{s}	Internal loss	5000 m^{-1}
n_{eff0}	Effective refractive index	3.2
n_{g}	Group refractive index	3.6
N_{T}	Transparent carrier density	1.5×10^{24} m^{-3}
α_m	Linewidth enhancement factor	1
Γ	Confinement factor	0.08
g_N	Differential gain	1.5×10^{5} /m
ε	Gain suppression coefficient	6×10^{-23} m^3
γ	Spontaneous emission coefficient	5×10^{-5}

Section 2: Experimental results for simultaneous implementation of neuron excitability threshold and synaptic linear weighting functions.

As depicted in Fig. 4(c) in the main text, the excitability threshold plasticity and linear weighting function was simultaneously achieved by simply modulating the gain current of the DFB-SA. The enlargement of a single period was further presented in Fig. S1.

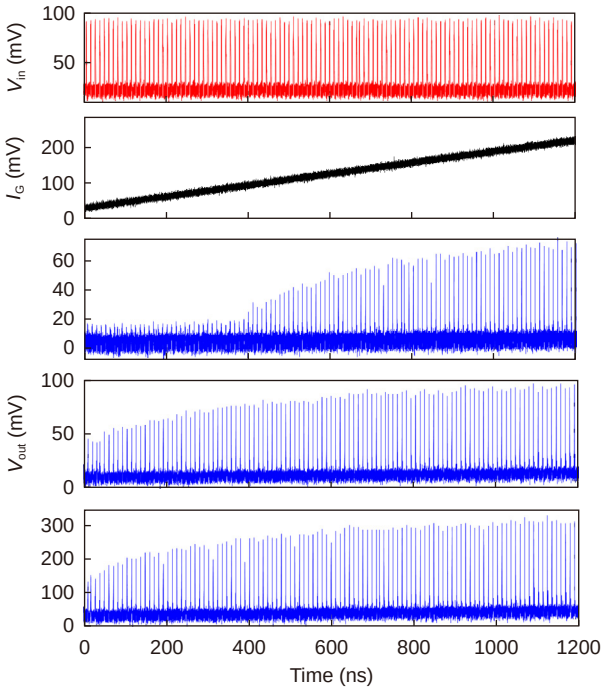

Fig. S1 | Experimental demonstration of simultaneous implementation of neuron excitability threshold and synaptic linear weighting functions for a continuously-varying gain current.

Section 3: Numerical results for simultaneous implementation of neuron excitability threshold and synaptic linear weighting functions

With the developed theoretical model of the DFB-SA, we performed numerical simulations to reproduce the results for the simultaneous implementation of neuron excitability threshold and synaptic linear weighting functions. The results are shown in Fig. S2, which agree well with the experimental findings.

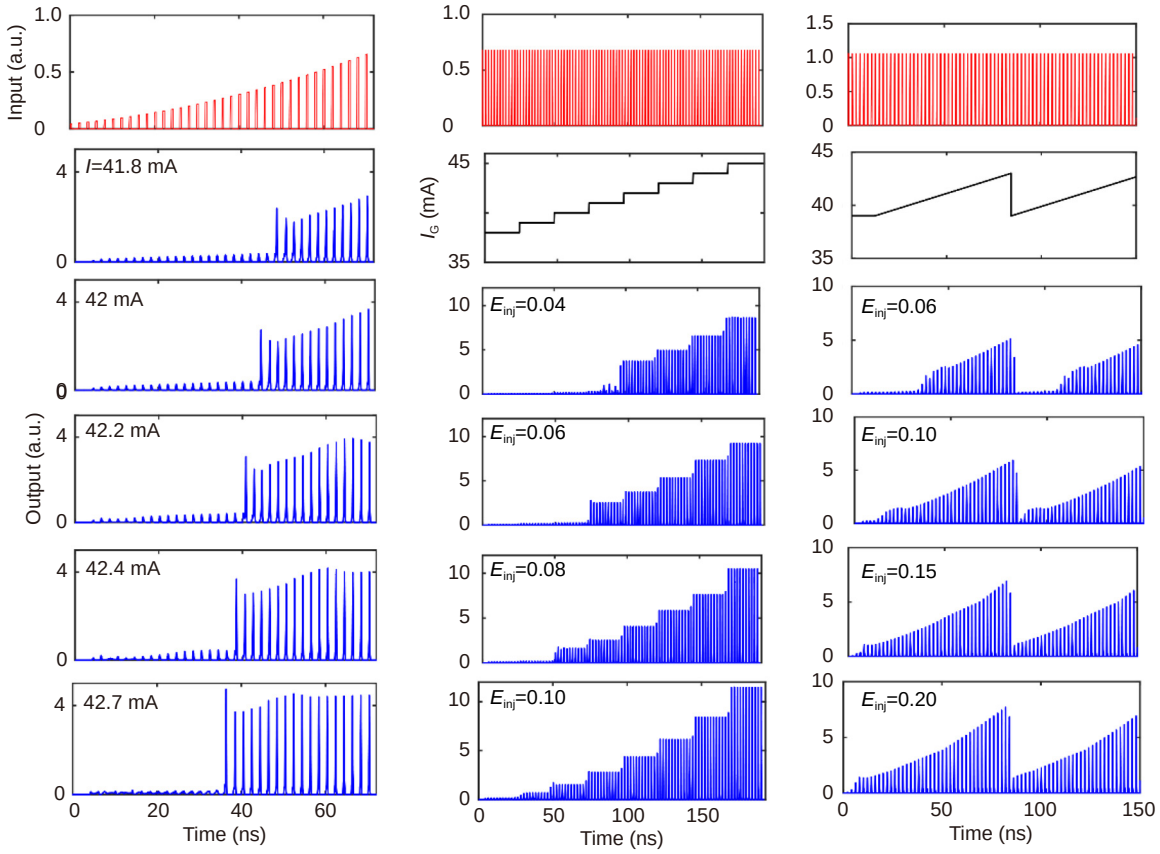

Fig. S2 | Numerical demonstration of simultaneous implementation of neuron excitability threshold and synaptic linear weighting functions in a single DFB-SA.

Section 4: The trained weights of 16 convolutional kernels for the convolutional layer.

The spiking CNN is trained with a digital computer. The surrogate gradient algorithm is employed to train the network. In the case of forward propagation, we use IF neurons for activation to increase the nonlinearity. However, due to the problem that the output of spiking neuron is not differentiable, we use softsign function, which is similar to the step function but differentiable, to replace the step function in the case of back propagation.

The four elements in a 2×2 convolution kernel matrix are respectively mapped to one DFB-SA. As depicted in Fig. S3, the trained weight values for each DFB-SA channel are represented by distinct colors.

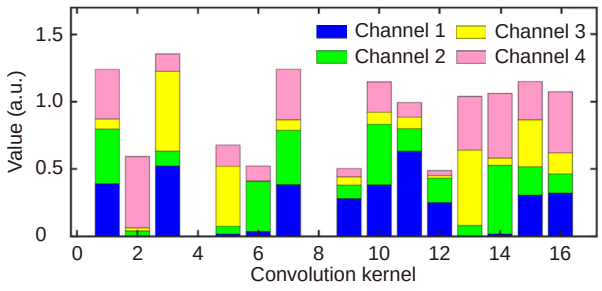

Fig. S3 | The distribution of weight values for 16 convolution kernels for each channel.

Section 5: Experimental measured optical spectra of the fabricated four-channel DFB-SA laser array.

In our experiments, the optical spectra for the four free-running DFB-SA lasers are presented in Fig. S4. The peak wavelength is 1553.18 nm, 1553.72 nm, 1554.22 nm, and 1554.74 nm.

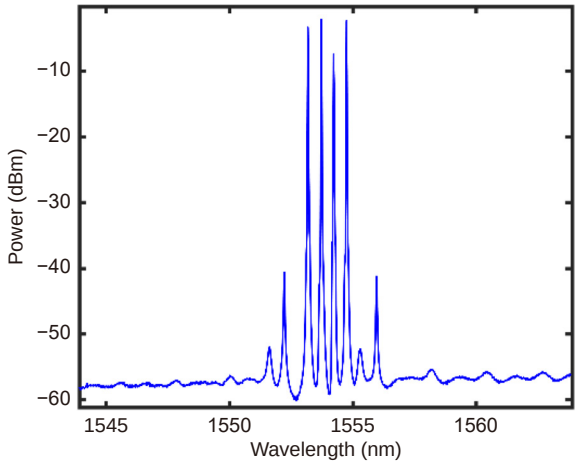

Fig. S4 | The optical spectra for the four-channel free-running DFB-SA lasers.

Section 6: Experimental results of temporal time series for some representative input samples.

In our experiments, we precisely adjusted the static gain current and reverse voltage of the SA region for four DFB-SA lasers to ensure that the same weight can be equally represented by different DFB-SA laser. The conditions are set as: DFB-SA1: V_{SA}=−0.8911 V, I_{G0}=64.5 mA; DFB-SA2: V_{SA}=−0.3812 V, I_{G0}=64.8 mA; DFB-SA3: V_{SA}=−1.4401 V, I_{G0}=84.1 mA; DFB-SA4: V_{SA}=−1.1214 V, I_{G0}=81.8 mA. Note, for each DFB-SA laser, the static gain current is combined with the modulated current denoting the kernel weight through a bias tee. The experimental measured temporal outputs of the weighted addition signal for ten representative input samples are illustrated in Fig. S5.

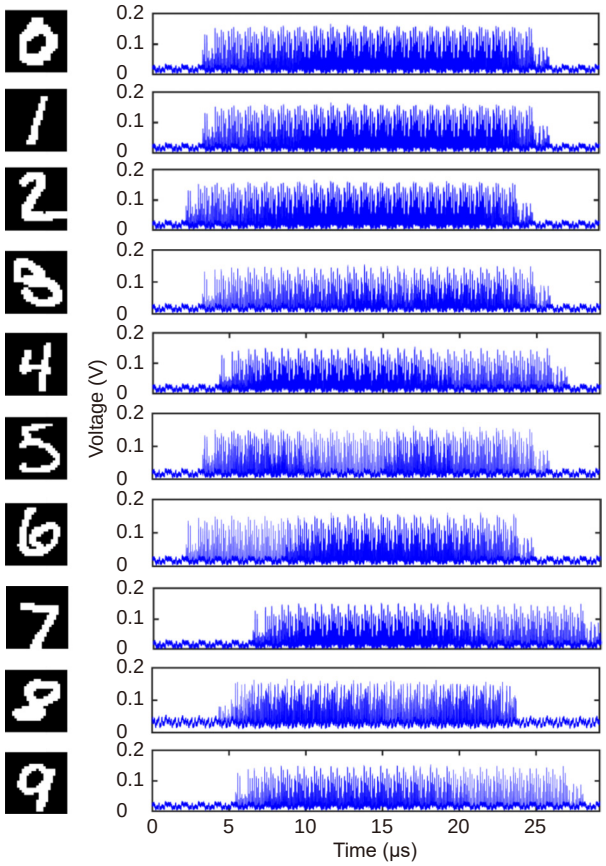

Fig. S5 | The experimental measured weighted addition signal for ten representative input samples.

Section 7: The feature maps recovered from the experimental results of temporal time series.

Here, we present the recovered feature map based on the measured temporal time series. To recover the feature maps, the maximum value for each pixel duration of 2.5 ns was extracted. Thus, 16 feature maps with a size of 27×27 pixels were obtained for each input image. In the displayed examples in Figs. S6–S8, the input images correspond to digits 9, 7, and 4, respectively.

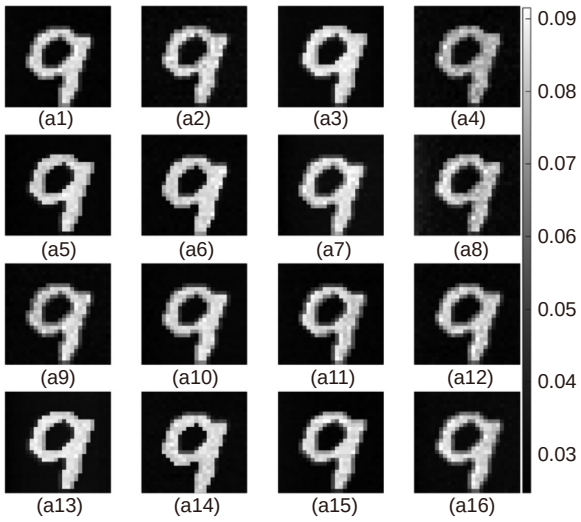

Fig. S6 | The feature maps recovered from the temporal outputs for 16 convolutional kernels corresponding to input sample of number 9.

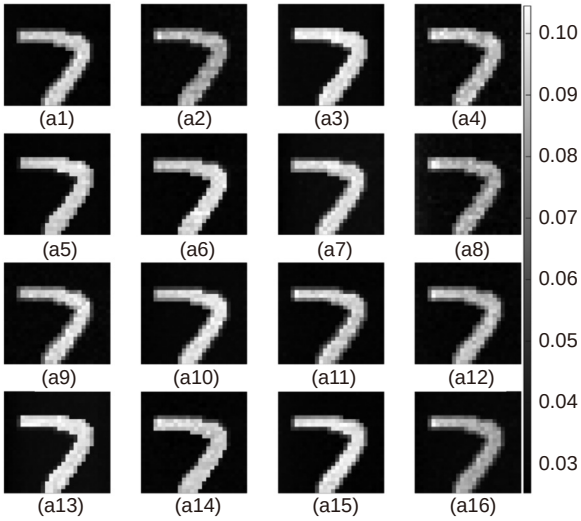

Fig. S7 | The feature maps recovered from the temporal outputs for 16 convolutional kernels corresponding to input sample of number 7.

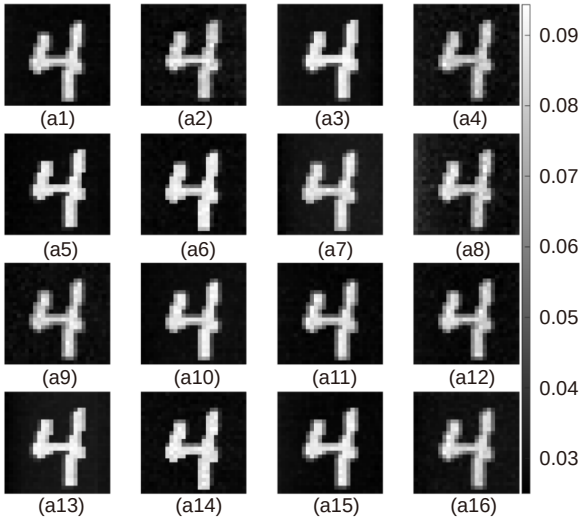

Fig. S8 | The feature maps recovered from the temporal outputs for 16 convolutional kernels corresponding to input sample of number 4.

Section 8: The numerical results of parallel dot product with an array of four DFB-SA lasers.

Based on the time-dependent traveling wave model developed for the DFB-SA laser, we simulated the case of a 2×2 convolution kernel by using an array of four DFB-SA lasers. The simulation results are presented in Fig. S9. From these numerical results, we can see that four-channel parallel time-varying linear weighting operation could be effectively realized with the four DFB-SA lasers.

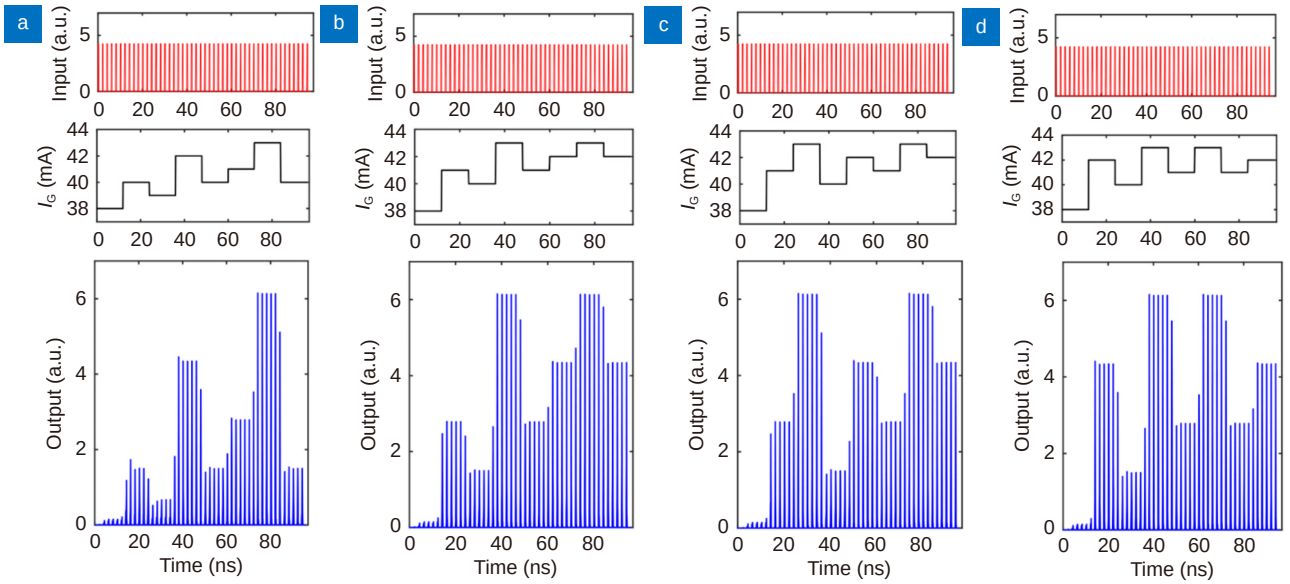

Fig. S9 | Numerical results of parallel linear weighting with a four-channel DFB-SA laser array.

Section 9: The numerical results of parallel dot product with an array of nine DFB-SA lasers.

The present DFB-SA laser array only contains four channels, which can support a convolution kernel with size of 2×2. It was demonstrated that the DFB laser array could be scaled up to 60 channels. Thus, the photonic neuro-synaptic core based on the DFB-SA laser array is scalable. Based on the time-dependent traveling wave model developed for the DFB-SA laser, we simulated the case of a 3×3 convolution kernel by using an array of nine DFB-SA lasers. The simulation results are presented in Fig. S10. For clarity, the input is considered as the same for each DFB-SA laser, while the modulation current applied to the gain region of each DFB-SA laser is distinct. It can be found that the linear weighting operation could be effectively realized in parallel with the nine DFB-SA lasers.

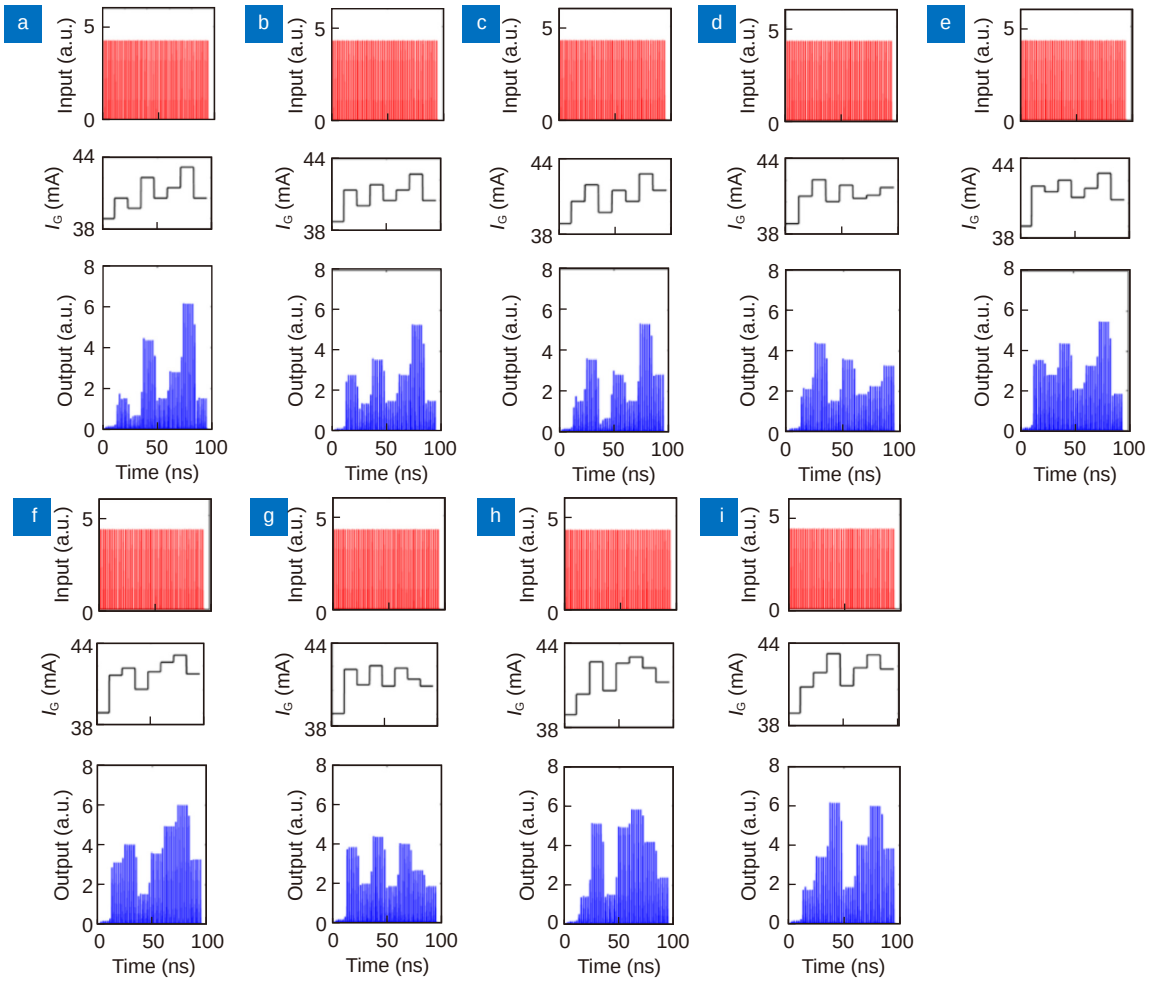

Fig. S10 | Numerical results of parallel linear weighting with a nine-channel DFB-SA array.

Section 10: Training accuracy and confusion matrix for a network with larger convolution kernel size.

We also consider a larger convolution kernel size. Similar to the network presented in the main text, the considered spiking CNN also comprises a convolutional layer with 16 @3×3 convolutional kernels, an activation layer, a pooling layer, and two fully-connected layers.

The training accuracy and confusion matrix are presented in Fig. S11. The inference accuracy is 92.45%.

Furthermore, we also consider a spiking CNN with two convolutional layers, two activation layers, two pooling layers, and two fully-connected layers. The convolutional kernels with size of 2×2 and 3×3 are both considered. The training accuracy and confusion matrix are presented in Fig. S12–S13 for size of 2×2 and 3×3, respectively. The inference accuracy is 93.76% and 94.42%. That is to say, more convolutional layers lead to higher inference accuracy.

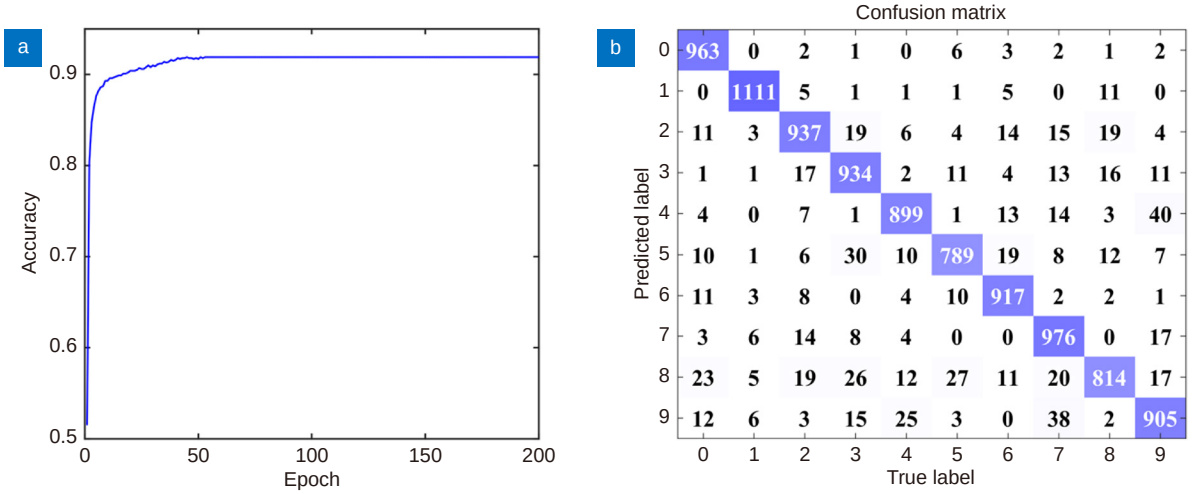

Fig. S11 | (**a**) Training accuracy and (**b**) confusion matrix for spiking CNN with 3×3 convolution kernel.

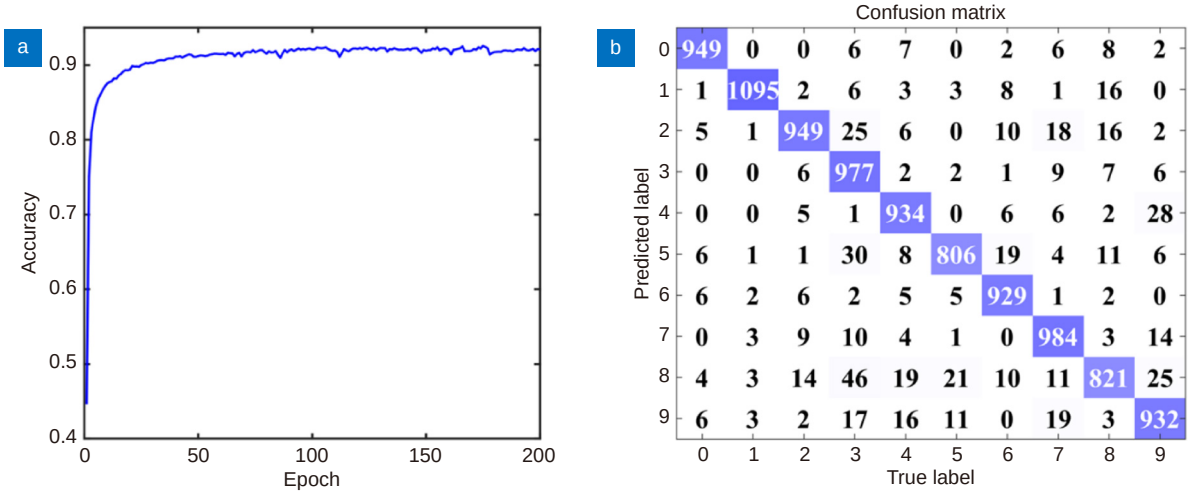

Fig. S12 | (**a**) Training accuracy and (**b**) confusion matrix for spiking CNN with two convolutional layers, with 2×2 convolution kernel.

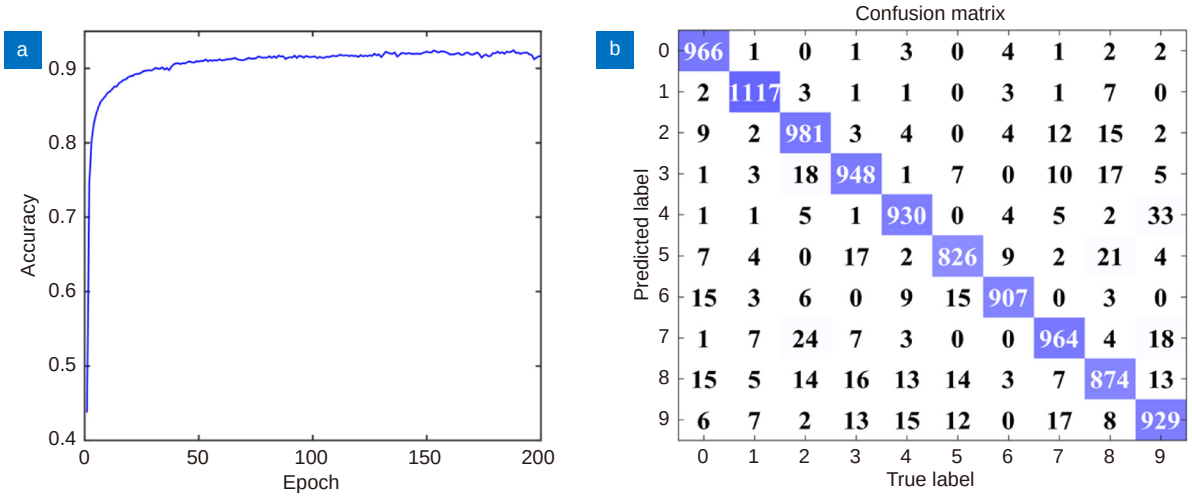

Fig. S13 | (**a**) Training accuracy and (**b**) confusion matrix for spiking CNN with two convolutional layers, with 3×3 convolution kernel.

References

S1. Zhao Y, Shi YC, Li J, Liu SP, Xiao RL et al. A cascaded tunable DFB semiconductor laser with compact structure. *IEEE J Quantum Electron* **54**, 2200111 (2018).

S2. Sun ZX, Xiao RL, Zhao Y, Lv G, Su ZR et al. Design of four-channel wavelength-selectable in-series DFB laser array with 100-GHz spacing. *J Lightw Technol* **38**, 2299–2307 (2020).

S3. Li X. *Optoelectronic Devices*: *Design*, *Modeling*, *and Simulation* (Cambridge University Press, Cambridge, 2009).

S4. Labukhin D, Stolz CA, Zakhleniuk NA, Loudon R, Adams MJ. Modified fabry–perot and rate equation methods for the nonlinear dynamics of an optically injected semiconductor laser. *IEEE J Quantum Electron* **45**, 863–871 (2009).